Comprehensive Diagnosis of Growth Rates of the Ablative Rayleigh-Taylor Instability

H. Azechi, T. Sakaiya, S. Fujioka, Y. Tamari, K. Otani, K. Shigemori, M. Nakai, H. Shiraga, N. Miyanaga, and K. Mima

Institute of Laser Engineering, Osaka University, 2-6 Yamada-oka, Suita, Osaka 565-0871, Japan

(Received 6 July 2006; published 24 January 2007)

The growth rate of the ablative Rayleigh-Taylor instability is approximated by $\gamma = \sqrt{kg/(1+kL)} - \beta k\dot{m}/\rho_a$, where k is the perturbation wave number, g the gravity, L the density scale length, $\dot{m}$ the mass ablation rate, and ρ_a the peak target density. The coefficient β was evaluated for the first time by measuring all quantities of this formula except for L, which was taken from the simulation. Although the experimental value of $\beta = 1.2 \pm 0.7$ at short perturbation wavelengths is in reasonably good agreement with the theoretical prediction of $\beta = 1.7$, it is found to be larger than the prediction at long wavelengths.

DOI: 10.1103/PhysRevLett.98.045002 PACS numbers: 52.35.Py, 52.50.Jm, 52.57.Fg, 52.70.La

The concept of inertial confinement fusion (ICF) is that a spherical pellet made of deuterium and tritium is imploded by irradiating the surface directly with high power lasers, ion beams, or soft x rays, thereby assembling a high-density main fuel and a hot spark triggering thermonuclear ignition [1]. Hydrodynamic instabilities such as the Rayleigh-Taylor (RT) instability [2,3] may potentially prevent the pellet from being compressed. Fortunately, in ICF targets, there exists material ablation through the unstable interface. It is believed that since the ablation removes the RT perturbation away from the unstable surface, the RT growth is significantly moderated. Such instability is called ''ablative RT instability''.

The growth rate γ of the ablative RT instability has been suggested by Bodner [4] and is approximated by the following Takabe-Bodner formula [5,6]:

$$\gamma = \sqrt{kg/(1+kL)} - \beta k\dot{m}/\rho_a, \quad (1)$$

where k is the perturbation wave number, g is the gravity, L is the density scale length at the ablation surface, $\dot{m}$ is the mass flux through the ablation surface (mass ablation rate), ρ_a is the peak target density, and the coefficient β is a complex function of the ablation structure. Betti *et al.* [7] have found an analytical solution that can be approximated by Eq. (1). They predict that the x-ray transport modifies the plasma density profile, resulting in $\beta = 1.7$ for plastic ICF targets. Kull and Anisimov [8], Sanz [9], and Piriz [10] also analytically found the similar formula of the RT growth rate.

Although a number of experimental data [11–18] have been compared with Eq. (1), there has been no experimental study to determine the value of β. This is due to the lack of diagnostic techniques to measure the ablation density and the density scale length. In order to resolve this problem, we have innovated high spatial resolution x-ray imaging techniques, such as penumbral x-ray imaging [19] and the Fresnel phase zone plate [20]. It finally becomes possible to evaluate the coefficient β by directly measuring all quantities (k, g, $\dot{m}$, ρ_a, and γ) of Eq. (1) except for the density scale length.

The schematic view of the experimental setup is shown in Fig. 1. The target was irradiated by a drive laser and was diagnosed with face-on and side-on radiography. The targets were made of polystyrene (CH) with a density of 1.06 g/cm^3 and a thickness of 40 μm. The laser irradiation side of the target was coated with 0.05 μm thick Al to prevent early laser penetration into the target. The drive laser was smoothed by two-dimensional and three-directional spectral dispersion (SSD) of 0.35 μm wavelength [21–23] which was preceded by the partially coherent light (PCL) of 0.53 μm wavelength [24,25] as a foot pulse. For further smoothing, kinoform phase plates [26] were implemented in front of the focusing lenses. The spot diameter was about 600 μm. The laser pulse shape of the foot (PCL) and the main (SSD) pulse was nearly flat top with full width at half maximum of 2.3 and 2.5 ns, respectively. The laser intensity of the foot and main pulse was 3×10^{12} and 7×10^{13} W/cm^2. Throughout this Letter we define the time zero ($t = 0$ ns) as a time of the first half maximum of the main pulse.

Sinusoidal perturbation on the surface of the CH target was imposed by Fourier laser machining [27] for the 20-μm perturbation wavelength and thermal press technique [28] for the 50-μm perturbation wavelength. The

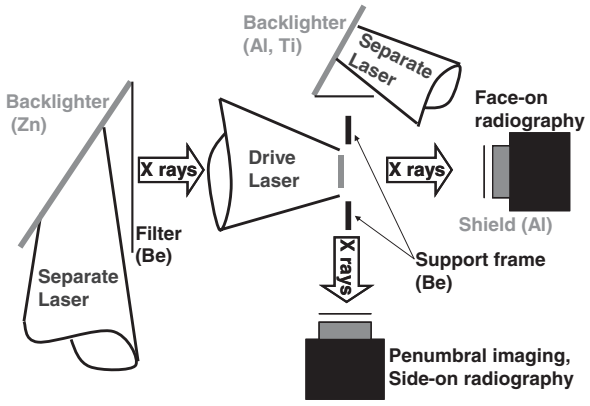

FIG. 1. The schematic view of the measurements of all quantities of Eq. (1).

amplitude of the higher harmonics mode was measured to be much smaller than that of the fundamental mode. The imposed perturbation wavelengths (amplitude) were 19.7 μm (0.176 μm) and 53.4 μm (0.249 μm).

The target density was obtained by observing the transmittance distribution with high-resolution x-ray penumbral imager with side-on radiography [19]. The blur both by the instrumental resolution (3 μm) and by the target motion (6 μm) during the x-ray flash (160 ps) was iteratively removed by fitting a calculated transmittance profile with the observed one. The peak target density and the density scale length at 1.5 ns are deduced to be $2.1^{+0.3}{}_{-0.2}$ g/cm^3 and $3.0^{+2.2}{}_{-1.0}$ μm, respectively. The detail of the procedure and the related error evaluation are described in Ref. [19]. In brief, a quadrature sum of the deduced target thickness (17 μm), the resolution, and the motion blurring suggests an increase of the thickness in appearance and hence a decrease of the density by about 10% relative to the actual values. This is consistent with the error of the density measurement. The measured density is well reproduced by the one-dimensional (1D) simulation code "ILESTA-1D" [29,30]. Although the density scale length has a large fractional error, it is still consistent with the 1D simulation of 1.5 ± 0.5 μm. The good agreement of the density and the consistency of the density scale length validate adopting the prediction of the density scale length.

The growth rate was obtained by observing the growth of the areal-density perturbation with face-on radiography using a Zn target as an x-ray source (~1.5 keV). We used a 10×50 μm^2 slit as an x-ray imager. The temporal resolution of the x-ray streak camera for the measurement is about 150 ps. The spatial resolution defined as the point where modulation transfer function (MTF) becomes 5% is 12 μm (This is much worse than that of the density measurement).

The result of the face-on radiography is shown in Fig. 2(a). It is observed that the contrast of the image increases with time due to the RT instability. The line scan data at various observation times is normalized by the spatial distribution of the transmitted x-ray intensity, which is obtained by fitting a polynomial function with the distribution of the observed data themselves. The normalized profile is then Fourier analyzed to give the amplitude of the fundamental mode. The areal-density perturbation amplitude is obtained from the amplitude of the fundamental mode divided by the mass absorption coefficient and by the MTF. Figures 2(b) and 2(c) show the time evolution of the growth factors, which is defined as the measured areal-density perturbation divided by the initial value. The error bar of the growth factor at various times is calculated from the fluctuation of the individual perturbation amplitude. The uncertainty of the MTF just adds a scale factor that drops out when one deduces a growth rate. The fluctuation of the linearity of the streak camera response is much smaller than the data fluctuation.

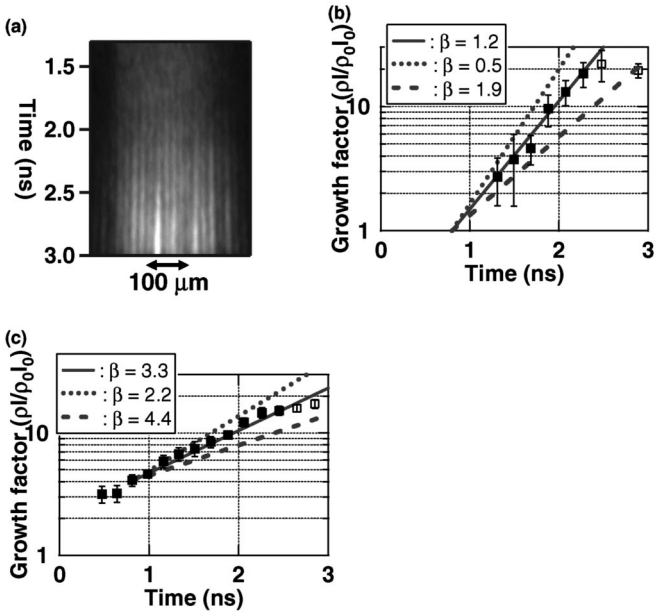

FIG. 2. (a) The raw images of the Rayleigh-Taylor experiment for the perturbation wavelength of 20 μm. The time evolution of the growth factor for (b) $\lambda = 20$ μm and (c) $\lambda = 50$ μm.

The growth rate of the RT instability and the error is obtained from the maximum likelihood estimation [31] where each data point is assumed to distribute around a true value determined from the fitted function with the growth rate and the initial areal-density perturbation as parameters. We used an exponential function as the fitted function for the data in a linear regime. It is defined as the time interval from the time at which the acceleration of the target begins (0.8–0.9 ns) to the earlier time of either the end of the acceleration or the beginning of the saturation of the RT growth. The data at $t = 2.5$ ns and later are discarded in the evaluation [open square data in Figs. 2(b) and 2(c)]. It is worthwhile to note that the fractional error of the growth rate is smaller than that of each individual datum since it is based on a fit of the full data set.

The target trajectory was measured with side-on radiography. The target for the x-ray source was an Al foil, producing 1.5–1.7 keV x rays. The slit as the x-ray imager was set so that the height direction was parallel to the target edge. The observed target trajectory is shown in Fig. 3(a). The target trajectory is obtained by plotting the peak attenuation point and displayed in Fig. 3(b). The error bars indicate the spatial width of the foil in the shadow. The bold curve shows the mass center of the target calculated from the 1D simulation. The experimental trajectory is in excellent agreement with the result of the 1D simulation. The gravity and the error are evaluated again with the maximum likelihood estimation. The fitted function is a second-order polynomial, where the initial velocity and its uncertainty are determined from the measured shock breakout time. The open square data were discarded in the evaluation because of no drive laser at these times.

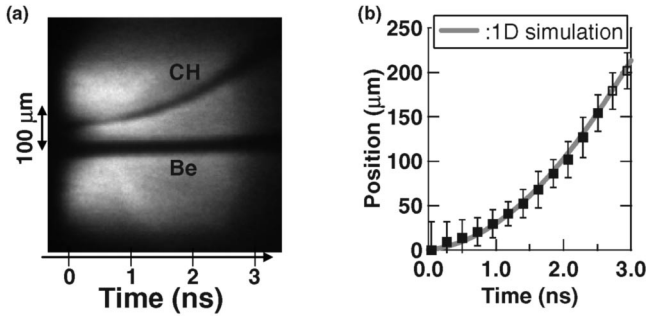

FIG. 3. (a) The raw image of the target trajectory measured with an x-ray streak camera. (b) The target trajectory as a function of time.

The mass ablation rate was measured from time-dependent x-ray transmittance with face-on radiography [32]. Since the ablated material is heated to ~keV temperature and hence fully ionized, the x-ray transmittance is solely due to the residual target mass. The time derivative of the residual mass gives the mass ablation rate. The observed image for the mass ablation rate measurement is shown in Fig. 4(a). The unattenuated (reference) x-ray intensity used to calculate the transmittance was determined from the intensity recorded past the edge of the target (left side of the image) combined with a separate spatially resolved measurement of the x-ray emission from the source. The temporal change of the x-ray transmittance is shown in Fig. 4(b), together with the simulation results with varying laser intensity by ±40%. The experimental result of the mass ablation rate is well reproduced by the 1D simulation. The slight stagnation of the transmittance at around $t = 1.2$ ns is due to the decrease of the laser intensity around that time. The mass ablation rate is obtained from the maximum likelihood estimation for the time development of the transmittance.

We summarize the experimental condition and result of the measured quantities in Table I. Since there is slight difference of the experimental condition at which each quantity was measured, some corrections of the data are made. We take the experimental condition (target thickness and laser intensity) of the growth rate measurement as a ''standard'' one, then the gravity and the mass ablation rate

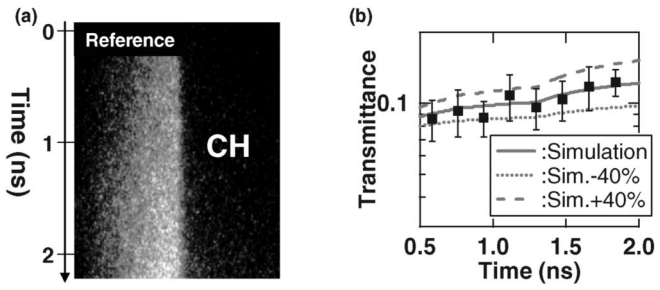

FIG. 4. (a) The raw image of the mass ablation rate measurement. (b) The time development of the transmittance.

at the standard condition are corrected by using a laser intensity scaling [33] of the pressure and the mass ablation rate, i.e., $P \propto I^{3/4}$, $\dot{m} \propto I^{1/2}$, and obvious relation of $g = P/m$, where P is the ablation pressure, I is the laser intensity, and m is the target areal density. Other intensity scaling, such as, $P \propto I^{2/3}$ and $\dot{m} \propto I^{1/3}$ [34] results in insignificant change of the value of β. Since the laser intensity for the growth rate measurement at the longer perturbation wavelength is almost the same as that for the density measurement, no correction is made for the density profile. Although the laser intensity is significantly higher for the growth rate measurement at the shorter perturbation wavelength, the peak density is calculated to be only 5% higher than that of the lower irradiance and the density scale length is calculated to be unchanged. We therefore make this slight correction to the peak density for the higher irradiance.

The value of β is evaluated from Eq. (1) with the physical parameters listed in Table I to be 1.2 ± 0.7 for $\lambda = 20$ μm and 3.3 ± 1.1 for $\lambda = 50$ μm. The error is evaluated from a standard error propagation theorem [35]. The curves in Fig. 2 illustrate the sensitivity of the growth factor to the value of β, that is varied from the lower to the higher boundaries. In this illustration, the initial perturbation amplitude is assumed to be equal to the measured or inferred growth factor at the time of the beginning of the acceleration ($t = 0.8$–0.9 ns). The deduced value of β for the shorter perturbation wavelength is consistent with the theoretical prediction [7] of $\beta = 1.7$, whereas that for the longer perturbation wavelength is excessively larger than the prediction. This provides the first rigorous test for the theory of the ablative RT instability.

As was suggested [18], the larger value of β at long wavelengths is possibly explained by the nonuniform ablation flow that modifies the laser-absorption region, thereby increasing the dynamic overpressure. In the concave region of the target, for example, the ablation flow blows the laser-absorption region far away from the target. In this region, the incoming laser is refracted out, and furthermore the energy flux is reduced due to the increased distance between the ablation and the absorption region, thereby reducing the ablation pressure. These effects tend to reduce the perturbation amplitude. Previous theories include the dynamic overpressure, but do not include its enhancement by the perturbation of the laser-absorption region.

In summary, the growth rates of the ablative Rayleigh-Taylor instability were comprehensively investigated. The coefficient β which indicates the effectiveness of the ablative stabilization was determined for the first time by directly measuring the gravity, the mass ablation rate, the peak target density, and the growth rate, while the value of the density scale length was taken from the simulation. At the short perturbation wavelength, the experimental value of $\beta = 1.2 \pm 0.7$ is well consistent with the theoretical prediction of $\beta = 1.7$. Contrary to the theoretical predic-

TABLE I. The values of all parameters of Eq. (1) which are obtained from the each experiment.

	Short wavelength	Long wavelength
Perturbation wave number (μm^{-1}	$2\pi/(19.7 \pm 0.1)$	$2\pi/(53.4 \pm 0.3)$
Intensity (TW/cm^2)	120	65
ρ_a (g/cm^3)	2.2 ± 0.3	2.1 ± 0.3
L (μm): Simulated	1.5 ± 0.5	1.5 ± 0.5
γ (ns^{-1})	2.0 ± 0.4	0.8 ± 0.1
$g(\times 10^{15}$ $cm/s^2)$	3.8 ± 0.5	2.2 ± 0.3
$\dot{m}(\times 10^5$ g/cm^2 s)	4.9 ± 0.9	3.7 ± 0.7
β	1.2 ± 0.7	3.3 ± 1.1

tion, however, the coefficient β is much larger at the long wavelength region.

We would like to acknowledge the dedicated technical support by the staff at the GEKKO XII facility for the laser operation, the target fabrication, and the plasma diagnostics. We would also like to acknowledge Prof. J. Sanz, Catedratico de Universidad, for his useful discussion. This work was supported by Japan Society for the Promotion of Science under the contract of Grant-in-Aid for Scientific Research (A) No. 14208048 and Grant-in-Aid on Priority Area No. 16082204.

[1] J. H. Nuckols *et al.*, Nature (London) **239**, 139 (1972).
[2] L. Rayleigh, Proc. London Math. Soc. **10**, 4 (1879); *Scientific Papers II* (Cambridge University Press, Cambridge, England, 1900), p. 200.
[3] G. I. Taylor, Proc. R. Soc. A **201**, 192 (1950).
[4] S. Bodner, Phys. Rev. Lett. **33**, 761 (1974).
[5] H. Takabe *et al.*, Phys. Fluids **28**, 3676 (1985).
[6] J. D. Lindl, Phys. Plasmas **2**, 3933 (1995).
[7] R. Betti *et al.*, Phys. Plasmas **5**, 1446 (1998).
[8] H. J. Kull and S. I. Anisimov, Phys. Fluids **29**, 2067 (1986).
[9] J. Sanz, Phys. Rev. Lett. **73**, 2700 (1994).
[10] A. R. Piriz, Phys. Plasmas **8**, 997 (2001).
[11] B. A. Remington *et al.*, Phys. Rev. Lett. **67**, 3259 (1991).
[12] K. Shigemori *et al.*, Phys. Rev. Lett. **78**, 250 (1997).
[13] H. Azechi *et al.*, Phys. Plasmas **4**, 4079 (1997).
[14] S. G. Glendinning *et al.*, Phys. Rev. Lett. **78**, 3318 (1997).
[15] C. J. Pawley *et al.*, Phys. Plasmas **6**, 565 (1999).
[16] J. P. Knauer *et al.*, Phys. Plasmas **7**, 338 (2000).
[17] K. Budil *et al.*, Phys. Plasmas **8**, 2344 (2001).
[18] T. Sakaiya *et al.*, Phys. Rev. Lett. **88**, 145003 (2002).
[19] S. Fujioka *et al.*, Phys. Plasmas **10**, 4784 (2003).
[20] Y. Tamari *et al.*, *Two-Dimensional Ablation Density Measurement Relevant to Rayleigh-Taylor Instability with Fresnel Phase Zone Plate, Sept. 7-12, 2003, Monterey, CA* (American Nuclear Society, LaGrange Park, IL, 2003), p. 182.
[21] S. Skupsky *et al.*, J. Appl. Phys. **66**, 3456 (1989).
[22] N. Miyanaga *et al.*, Proc. SPIE-Int. Soc. Opt. Eng. **3047**, 746 (1997).
[23] G. Miyaji *et al.*, Opt. Lett. **27**, 725 (2002).
[24] H. Nakano *et al.*, Appl. Phys. Lett. **63**, 580 (1993).
[25] K. Mima *et al.*, Phys. Plasmas **3**, 2077 (1996).
[26] S. N. Dixit *et al.*, Opt. Lett. **19**, 417 (1994).
[27] T. Sakaiya, Ph.D. thesis, Osaka University, Osaka, Japan, 2005.
[28] K. Shigemori, M. Takagi, and H. Azechi, *Annual Progress Report of Institute of Laser Engineering* (Osaka University, Osaka, Japan, 1995), p. 135.
[29] H. Takabe *et al.*, Phys. Fluids **31**, 2884 (1988).
[30] A. Sunahara *et al.*, Phys. Rev. Lett. **91**, 095003 (2003).
[31] W. H. Press *et al.*, *Numerical Recipes in C++* (Cambridge University Press, New York, 2002), Chap. 15. Assuming a normal distribution of each data point around the true value, we can get the probability P for the growth rate as $P(\gamma, h_0) = \prod_{i=1}^{N}\{\exp[-\frac{1}{2}(\frac{y_i - y(t_i,\gamma,h_0)}{\sigma_i})^2]\}$, where N is the number of the data, y_i the data of the areal-density perturbation, $y(t_i, \gamma, h_0)$ the fitted function with the growth rate γ and the initial areal-density perturbation h_0 as a fitting parameter, and σ_i the error of each datum. The standard deviation of P as a function of γ gives the error σ_γ, where we allow all potential h_0.
[32] K. Shigemori *et al.*, Rev. Sci. Instrum. **69**, 3942 (1998).
[33] P. Mora, Phys. Fluids **25**, 1051 (1982).
[34] W. M. Manheimer, D. G. Colombant, and J. H. Gardner, Phys. Fluids **25**, 1644 (1982).
[35] G. F. Knoll, *Radiation Detection and Measurement* (John Wiley & Sons, New York, 2000), Chap. 3, Sec. 4. Applying the error propagation formula on β of Eq. (1) gives $(\sigma_\beta/\beta)^2 = (\sigma_{\rho_a}/\rho_a)^2 + (\gamma_{\rm cl}/2\beta k v_a)^2[k\sigma_L/(1+kL)]^2 + (\gamma/\beta k v_a)^2(\sigma_\gamma/\gamma)^2 + (\gamma_{\rm cl}/2\beta k v_a)^2(\sigma_g/g)^2 + (\sigma_{\dot{m}}/\dot{m})^2$, where σ is the standard deviation of each subscript quantity, $\gamma_{\rm cl} \equiv \sqrt{kg/(1+kL)}$ is the classical growth rate, and $v_a \equiv \dot{m}/\rho_a$ the ablation velocity. The small uncertainty of k is ignored.